

Conserving Diagrammatic Approximations for Quantum Impurity Models: NCA and CTMA

J. KROHA¹ * and P. WÖLFLE² †

¹*Physikalisches Institut, Universität Bonn, 53115 Bonn, Germany*

²*Institut für Theorie der Kondensierten Materie, Universität Karlsruhe, 76128 Karlsruhe, Germany*

Self-consistent diagrammatic approximations to the Anderson or Kondo impurity model, using an exact pseudoparticle representation of the impurity states, are reviewed. We first discuss the infrared exponents of the pseudoparticle propagators as indicators of Fermi liquid behavior through their dependence on the impurity occupation and on magnetic field. Then we discuss the Non-Crossing Approximation (NCA), identifying its strengths, but also its fundamental shortcomings. Physical arguments as well as a perturbative renormalization group analysis suggest that an infinite parquet-type resummation of two-particle vertex diagrams, the Conserving T-Matrix Approximation (CTMA) will cure the deficiencies of NCA. We review results on the pseudoparticle spectral functions, the spin susceptibility and the impurity electron spectral function, supporting that the CTMA provides qualitatively correct results, both in the high-temperature regime and in the strong coupling Fermi liquid regime at low temperatures.

KEYWORDS: Kondo effect, Anderson impurity model, conserving approximations, Non-Crossing Approximation, Conserving T-Matrix Approximation, perturbative renormalization group

1. Introduction

Over the last 40 years the Kondo problem has become an archetypical model of correlated electrons. The discovery by Kondo¹ of logarithmic anomalies in the perturbation series for the electrical resistivity calculated within the spin exchange model of a magnetic impurity in a metal gave but the first indication of the existence of complex many-body effects in this and similar models. The key ingredient of these models is the availability of local degrees of freedom at the impurity, e.g. the substates of a local spin. Coupling of the quantum impurity to the conduction electrons of the metallic host induces a local interaction between the conduction electrons, and generates delicate many-body resonance states at low energy.

Soon after Kondo's discovery it became clear that perturbation theory in the antiferromagnetic exchange coupling constant J is sufficient only at high excitation energies/temperatures T so that $JN_0 \ln(D/T) \ll 1$, where $N_0 = \frac{1}{2D}$ is the conduction electron density of states at the Fermi level and D the half bandwidth (high-energy cutoff). By summing up the leading logarithmic terms to all orders of perturbation theory, using the perturbative renormalization group (RG) approach² it is found that a single dynamically generated energy scale, the Kondo temperature $T_K \approx D \exp -\frac{1}{2N_0J}$ is generated. The perturbative RG holds as long as $\ln(T/T_K) \gtrsim 1$.

In the opposite limit of $T \ll T_K$, the impurity spin is found to be screened by the conduction electron spins, and in the case of impurity spin $S = \frac{1}{2}$ coupled to a single band of conduction electrons, a spin singlet resonance state is formed. This has been established first beyond doubt within the numerical renormalization group method (NRG) pioneered by K.G. Wilson.³ Later an an-

alytical solution of the energy spectrum of the Kondo model was obtained with the aid of the Bethe ansatz (BA),^{4,5} fully confirming the NRG results.

While these highly successful exact solution methods have led to a virtually complete understanding of the single-impurity Kondo problem, it became clear in the course of the mid 1980s and 1990s that the Kondo-like enhancement of electron scattering at low energies plays a central role even in more complex situations, like in strongly correlated lattice electron systems as well as in mesoscopic devices. In the former systems, this is because the strong on-site repulsion in conjunction with a very short correlation length effectively induces local moment physics, as has been shown formally by the mapping of correlated lattice models onto quantum impurity models with a self-consistency condition by means of the Dynamical Mean Field Theory (DMFT).⁶ In the latter systems, discrete, localized quantum degrees of freedom, coupled to a continuum of conduction electrons, are often formed because of the spatial confinement of interacting electron states, e.g. in quantum dots⁸ and carbon nanotubes,⁹ nanoscale constrictions and charge traps,¹⁰ or magnetic molecules,¹¹ leading to Kondo behavior in the electronic transport. All these findings have demonstrated that the Kondo effect is an ubiquitous phenomenon in interacting electron systems and have made it a central theme of condensed matter physics.

To tackle the complex quantum impurity problems arising in such systems, it is desirable to develop, besides the exact solution methods, flexible, approximate, but systematic techniques which do not rely on special symmetry conditions or a relatively simple model structure, like NRG, or on integrability conditions, like the BA, and which are still capable of describing the high energy and low energy sectors of the model as well as the crossover region around T_K . In many respects, advanced

*E-mail Address: kroha@th.physik.uni-bonn.de

†E-mail address: woelfle@itkm.physik.uni-karlsruhe.de

perturbation theory methods are attractive here because of their flexibility. They do not require a simple conduction electron density of states (CDOS), and thus may be employed as impurity solvers for the self-consistent quantum impurity models of DMFT,⁶ where the CDOS may acquire considerable structure, e.g. a Mott-Hubbard gap and a narrow resonance in the gap. They may be applied to impurity models with more complex structure, e.g. Anderson models with several levels and realistic electron-electron interactions. They may even be used to describe quantum frustrated systems like multi-channel Kondo or Anderson models. An additional advantage of a method based on resummation of perturbation theory is that it may be easily generalized to nonequilibrium systems.^{13,36} The latter is of interest in the context of electron transport through nanostructures like quantum dots or point contacts showing the Kondo effect.

The perturbation theory for Kondo or Anderson models is complicated by the fact that the spin operators do not obey canonical commutation rules or that the electron dynamics on the Anderson impurity are effectively restricted to single occupancy by the strong Coulomb repulsion, respectively. This difficulty can be overcome efficiently by representing the quantum impurity degrees of freedom by canonical auxiliary particle fields,^{14,15} rendering Wick's theorem valid. For a description of the strongly correlated Fermi liquid (FL) ground state an infinite resummation of the logarithmic terms of perturbation theory is clearly necessary, where, however, the correct selection of terms is crucial. As will be seen, this can be achieved systematically by means of conserving approximations, derived by functional derivative from a generating functional.

In the present article we review the method of conserving approximations for Kondo-like models in terms of auxiliary particle fields, with special emphasis on describing, by means of a single approximation scheme, the perturbative regime at high energies as well as the strong coupling regime below T_K . We review the Non-Crossing Approximation (NCA) as the simplest of a hierarchy of conserving approximations and discuss its strengths and its fundamental failures. A detailed analysis will reveal the origins of the latter. This will lead to the Conserving T-Matrix Approximation (CTMA), which will be demonstrated to remedy the shortcomings of the NCA both in the high-energy and in the low-energy strong coupling regime.

2. Model and renormalized perturbation theory for constrained dynamics

In many situations the Kondo physics is more clearly described in terms of the Anderson impurity model,⁷

$$H = \sum_{\vec{k}\sigma} \epsilon_{\vec{k}} c_{\vec{k}\sigma}^\dagger c_{\vec{k}\sigma} + \sum_{\sigma} (\epsilon_d - \sigma B/2) d_{\sigma}^\dagger d_{\sigma} \quad (1)$$

$$+ V \sum_{\vec{k}\sigma} (c_{\vec{k}\sigma}^\dagger d_{\sigma} + h.c.) + U d_{\uparrow}^\dagger d_{\uparrow} d_{\downarrow}^\dagger d_{\downarrow}$$

where $c_{\vec{k}\sigma}^\dagger$ and d_{σ}^\dagger are the creation operators for electrons with spin $\frac{1}{2}$ (spin degree of freedom $\sigma = \pm 1$) in

a conduction band state \vec{k} and in the impurity level ϵ_d , respectively. To be general, we have included a magnetic field B acting on the impurity spin with Zeeman energy $B = g\mu_B \mathcal{B}$ (μ_B and g are the Bohr magneton and the Landé factor, respectively). The electrons may hop from the conduction band onto and off the impurity with amplitude V . A sufficiently large Coulomb interaction U at the impurity essentially prevents double occupancy of the impurity. Provided that the impurity level is sufficiently far below the Fermi energy E_F , its occupation number will be close to one, meaning that a spin $S = \frac{1}{2}$ is located at the impurity. The Kondo spin exchange interaction model follows from the Anderson model in the limit of nearly single electron occupancy, after projecting out the high energy sector.¹⁶

Since $V/D \ll 1$ usually, it appears natural to employ perturbation theory in V . This perturbation theory is complicated by two facts: (a) the impurity is an interacting electron system, for which the powerful quantum field theoretical methods like Wick's theorem, Feynman diagrams and renormalization of propagators and vertices are not immediately available; (b) the perturbation theory in V is characterized by logarithmically diverging terms, like the ones in the exchange coupling J .

2.1 Pseudoparticle representation

Problem (a) may be circumvented by working with pseudoparticle representations for the impurity states¹⁵ (or equivalently a resolvent operator formalism),

$$d_{\sigma}^\dagger = f_{\sigma}^\dagger b + \sigma a^\dagger f_{-\sigma}, \quad (2)$$

where f_{σ}^\dagger is the fermionic creation operator for the singly occupied impurity state with spin σ and b^\dagger , a^\dagger are the bosonic creation operators for the empty and doubly occupied impurity state, respectively. Since the pseudoparticle representation necessarily enlarges the Hilbert space into unphysical regions, care has to be taken to project onto the physical subspace, defined by all many-body states with pseudoparticle number $Q = \sum_{\sigma} f_{\sigma}^\dagger f_{\sigma} + b^\dagger b + a^\dagger a = 1$. This can be done in an elegant way for any expectation value of physical operators acting on the impurity states by working in the grand canonical ensemble with respect to the conserved charge Q and simply taking the negative chemical potential λ of the pseudoparticles to infinity^{14,15} at the end of the calculation, e.g. for the impurity or d -electron Green's function in the imaginary time domain,

$$G_{d\sigma}(\tau) = - \lim_{\lambda \rightarrow \infty} \frac{\langle d_{\sigma}(\tau) d_{\sigma}^\dagger(0) e^{-\beta[H + \lambda(Q-1)]} \rangle}{\langle Q e^{-\beta[H + \lambda(Q-1)]} \rangle}. \quad (3)$$

Since $\langle \dots \rangle$ denotes the (time ordered) *grand canonical* average with respect to Q , this procedure allows the use of the full machinery of quantum field theory, including Wick's theorem. It is worth pointing out that the representation Eq. (2) with the constraint $Q = 1$ enforced by Eq. (3) is exact. Physically observable quantities are necessarily given by two pseudoparticle (or higher) correlation functions, which in principle requires the calculation of both, self-energy and vertex corrections.

Inspection of the terms of perturbation theory shows that each contour integral along the branch cut of a pseu-

doparticle propagator carries a fugacity factor $e^{-\beta\lambda}$ and, thus vanishes in the limit $\lambda \rightarrow \infty$. As a consequence, any bubble diagram consisting only of pseudoparticle propagators vanishes in the physical subspace $Q = 1$, and any conduction electron propagator $G_{c\sigma}(\omega)$ appearing within an impurity diagram is not renormalized by the hybridization. Only in an expectation value of impurity operators like Eq. (3), one factor $e^{-\beta\lambda}$ is cancelled by a corresponding factor in $\langle Qe^{-\beta[S+\lambda(Q-1)]} \rangle$, leaving a single pseudoparticle bubble. Details of the evaluation of pseudoparticle diagrams can be found in Ref.¹⁷

2.2 Exact properties of the pseudoparticle propagators

The pseudoparticle propagators $G_x(\omega)$, $x = f\sigma, b, a$, are given in terms of the respective selfenergies $\Sigma_x(\omega)$ as

$$G_x(\omega) = [G_x^0(\omega)^{-1} - \Sigma_x(\omega)]^{-1}, \quad (4)$$

where the unrenormalized propagators read, after projection, $G_{f\sigma}^0(\omega) = [\omega - (\sigma + 1)B/2]^{-1}$, $G_b^0(\omega) = [\omega + \epsilon_d - B/2]^{-1}$, and $G_a^0(\omega) = [\omega - B/2 - U]^{-1}$. We now derive their exact low-energy behavior. Rewriting Eq. (3) in terms of pseudoparticle operators and using Wick's theorem, it is seen that in $G_x(\omega)$ the average $\langle \dots \rangle$ is confined to the $Q = 0$ sector because of the limit $\lambda \rightarrow \infty$. This implies that the pseudoparticle propagators have only forward in time propagation. Therefore, these propagators are similar to the propagators of the X-ray threshold problem, i.e. their spectral functions $A_x(\omega) = -\frac{1}{\pi} \text{Im} G_x(\omega + i0)$ show infrared threshold power-law behavior,

$$A_x(\omega) \sim \Theta(\omega) \omega^{-\alpha_x}, \quad x = f\sigma, b, a \quad \omega \ll T_K. \quad (5)$$

The exact infrared exponents α_x can be determined for the spin-screened (FL) case by the observation that in the X-ray problem they are related to the scattering phase shift $\delta_\sigma^{(x)}$ via $\alpha_x = 1 - \sum_\sigma \left(\delta_\sigma^{(x)} / \pi \right)^2$ and by employing the Friedel sum rule.^{18,19} It links the conduction electron number in channel σ , attracted from infinity in order to screen the impurity, to the phase shift, $\Delta n_{c\sigma}^{(x)} = \delta_\sigma^{(x)}$. $\Delta n_{c\sigma}^{(x)}$ in turn is defined as the difference between the average impurity occupation number $n_{d\sigma}$ in the stationary limit (time $t \rightarrow \infty$) and the impurity charge created by the respective pseudoparticle operator, f_σ^\dagger , b^\dagger , or a^\dagger at $t = 0$. Hence, we have for $G_{f\sigma}$: $\Delta n_{c\sigma}^{(f)} = n_{d\sigma} - 1$, $\Delta n_{c\sigma'}^{(f)} = n_{d\sigma'}$, $\sigma' \neq \sigma$; for G_b : $\Delta n_{c\sigma}^{(b)} = n_{d\sigma}$, and for G_a : $\Delta n_{c\sigma}^{(a)} = n_{d\sigma} - 1$, $\sigma = \pm 1$. This implies the exact values for the infrared exponents,²⁰ valid in the low-frequency regime $\omega < T_K$,

$$\alpha_{f\sigma} = n_d - n_d^2/2 + \Delta n_{d\sigma}(B) - \Delta n_{d\sigma}(B)^2/2 \quad (6)$$

$$\alpha_b = 1 - n_d^2/2 - \Delta n_{d\sigma}(B)^2/2 \quad (7)$$

$$\alpha_a = -1 + 2n_d - n_d^2/2 - \Delta n_{d\sigma}(B)^2/2, \quad (8)$$

where $n_d = \sum_\sigma n_{d\sigma}$ is the total impurity occupation number and $\Delta n_{d\sigma}(B) = n_{d\sigma} - n_{d-\sigma}$ the difference between the $\sigma = 1$ and $\sigma = -1$ occupation numbers in a magnetic field. The dependence of the exponents on n_d and $\Delta n_d(B)$ is characteristic for (FL) behavior because of the use of the Friedel sum rule (i.e. potential scattering

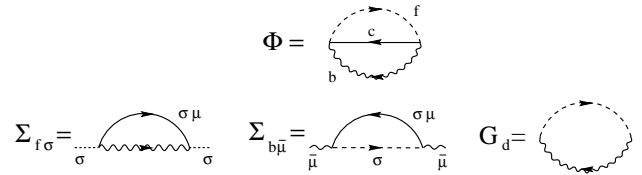


Fig. 1. Diagrammatic representation of the Luttinger-Ward functional generating the NCA for $U \rightarrow \infty$ and the corresponding pseudoparticle selfenergies $\Sigma_{f\sigma}$, Σ_b and the impurity electron Green's function $G_{d\sigma}$. Solid, dashed, and wiggly lines represent the conduction electron, the pseudofermion and the slave boson propagators, respectively. Throughout this paper, all lines are understood as the renormalized propagators, unless stated otherwise.

only) in their derivation. Therefore, whether or not the exponents are reproduced by a given approximation can serve as an indicator of its correctness, telling whether the approximation captures the spin-screened (FL) fixed point of the single-channel Anderson model. In the following we will focus mostly on the case of an infinite Coulomb repulsion U , where the more than singly occupied states (a, a^\dagger) do not contribute.

2.3 Conserving approximations

The solution to problem (b) requires the selection and summation of the essential terms of perturbation theory, in pseudoparticle representation. Precondition for the projection onto the physical subspace is the conservation of the local charge Q , implied by the symmetry with respect to simultaneous $U(1)$ gauge transformations of the pseudoparticles. Any approximation conserving the projection has to preserve gauge symmetry. This is achieved by constructing conserving approximations from a generating Luttinger-Ward functional Φ .²¹ The pseudoparticle selfenergies Σ_x are obtained as functional derivatives of Φ with respect to the corresponding Green's functions G_x , and are thus functionals of the dressed G_x . In this way a closed set of nonlinear coupled integral equations for the G_x 's is obtained for any choice of Φ . The choice of Φ furthermore dictates the calculation of the physical impurity electron Green's function $G_{d\sigma}$ (and other correlation functions), since, by definition, $|V|^2 G_{d\sigma} = \lim_{\lambda \rightarrow \infty} \delta\Phi / \delta G_{c\sigma}$ is the single-particle conduction electron T-matrix.

3. Non-Crossing Approximation

In view of the small parameter V/D it appears reasonable to start with the lowest (2nd order in V) approximation for Φ . Since in this approximation, which sums up infinitely many self-energy insertions, the corresponding Feynman diagrams do not have any crossings, it has been termed the "Non-Crossing Approximation" (NCA) (see Fig. 1). The NCA has been pioneered by Keiter and Kimball using the resolvent operator formalism^{22,23} and by Kuramoto, who first recognized the conserving nature of the NCA.²⁴ It took more than 10 years, before the NCA equations were numerically evaluated^{25,26} and further-more solved analytically in the limit of low energies at $T = 0$.²⁷ Most of these works were concerned with the limit of infinitely strong Coulomb interaction $U \rightarrow \infty$,

in which double occupancy of the impurity is strictly excluded. In this case, the selfconsistent NCA equations in conjunction with Eq. (4) read (compare Fig. 1),

$$\Sigma_{f\sigma}^{NCA}(\omega) = \Gamma \int \frac{d\varepsilon}{\pi} f(\varepsilon) A_{c\sigma}^0(-\varepsilon) G_b(\omega + \varepsilon) \quad (9)$$

$$\Sigma_b^{NCA}(\omega) = \Gamma \sum_{\sigma} \int \frac{d\varepsilon}{\pi} f(\varepsilon) A_{c\sigma}^0(\varepsilon) G_{f\sigma}(\omega + \varepsilon) \quad (10)$$

$$G_{d\sigma}^{NCA}(\omega) = \int d\varepsilon e^{-\beta\varepsilon} [G_{f\sigma}(\omega + \varepsilon) A_b(\varepsilon) - A_{f\sigma}(\varepsilon) G_b(\varepsilon - \omega)] , \quad (11)$$

where ω is understood as $\omega \pm i0$ for the retarded/advanced functions, $\Gamma = \pi N_0 |V|^2$, and $A_{c\sigma}^0 = \frac{1}{\pi} \text{Im} G_{c\sigma}^0 / N_0$ is the local conduction electron density of states per spin, normalized to the density of states at the Fermi level N_0 , and $f(\varepsilon) = 1/(\exp(\beta\varepsilon) + 1)$ is the Fermi distribution function. For $U \rightarrow \infty$ the NCA captures correctly the Kondo energy scale, and it provides a qualitative description of the formation of the Kondo resonance. However, it fails in a magnetic field even in the high temperature regime $T \gg T_K$, producing a spurious resonance in the impurity spectrum at $\omega = 0$, in addition to the two Zeeman-split Kondo peaks. The origin of this failure will be traced in the appendix by means of an RG analysis. The NCA fails furthermore at temperatures $T \ll T_K$, where spurious infrared singular behavior in physical quantities appears, in contradiction to the expected (FL) behavior.^{17,26,27} The infrared exponents of the auxiliary particle propagators come out independent of n_d , $\alpha_f^{NCA} = 1/(N+1)$, $\alpha_b^{NCA} = N/(N+1)$, with N the spin degeneracy, again in contrast to the FL behavior Eqs. (6–8). The low- T failure of NCA is less pronounced in $SU(N)$ symmetric models with $N \gg 1$. NCA becomes formally exact in the limit $N \rightarrow \infty$, with deviations appearing in $O(\frac{1}{N^2})$.^{26,28} Note that the deviation of the approximate NCA values for the pseudoparticle exponents α_f, b is of order $1/N$, not $1/N^2$ as one may have expected.

At finite Coulomb interaction U , the exchange interaction J acquires contributions from both, virtual excitations to the empty and to the doubly occupied impurity states. A simple generalization of NCA to this case, i.e. adding the second order perturbation theory for the two processes, fails to capture the simultaneous contribution of both channels in each order of bare perturbation theory, and therefore leads to a possibly by orders of magnitude incorrect value of T_K (in the worst case it is off by a factor of T_K/D). An infinite summation of vertex corrections (the symmetrized finite U NCA, or SUNCA) is necessary to cure this problem.²⁹

The failure of the NCA at temperatures $T \ll T_K$ can be traced back to its insufficient inclusion of coherent multiple spin-flip processes. The latter are responsible for the formation of the Kondo resonance state. A qualitative improvement therefore requires to include the proper vertex corrections which account for the dominant spin and charge fluctuations. There is strong evidence that this is achieved by the so-called Conserving T-Matrix Approximation (CTMA).^{19,30} Before we dis-

cuss the CTMA in section 6, we will in the next two sections present relatively easily tractable generalizations of the NCA to adapt problems with several local orbitals and with a large, but finite Coulomb repulsion U .

4. Multi-orbital Anderson impurity systems

In contrast to analytical and numerical, exact solution methods, the conserving technique is generalizable in a straight-forward way for impurity models with several local orbitals. Such problems arise, for instance, in cluster extensions of the DMFT,^{33,34} but also in transition and rare earth metal impurity systems. To give an understanding of the wealth of the low-energy spectra of such systems, we here treat, on the level of NCA, a Ce impurity embedded in a metallic host, for which experimental photoemission spectra are available.³⁵ Although the compound CeCu_2Si_2 is a heavy fermion lattice system, for which one expects in the lattice-coherent low- T state a dispersion of the Kondo quasiparticle resonance with width of order of T_K , the photoemission measures the momentum integrated spectral density (implying only a slight broadening of the observed resonance), so that direct comparison with the results of the impurity model are possible.

Ce has seven 4f orbitals, which are spin-orbit (SO) and crystal-field (CF) split and have an overall valence of close to 1 in CeCu_2Si_2 . Hence, one can assume a large on-site Coulomb repulsion $U \rightarrow \infty$ between all 4f orbitals, and the model Hamiltonian reads in auxiliary particle representation,

$$H = \sum_{\vec{k}\sigma} \epsilon_{\vec{k}} c_{\vec{k}\sigma}^\dagger c_{\vec{k}\sigma} + \sum_{m\sigma} \epsilon_{dm} f_{m\sigma}^\dagger f_{m\sigma} \quad (12)$$

$$+ \sum_{m\vec{k}\sigma} V_m (c_{\vec{k}\sigma}^\dagger b^\dagger f_{m\sigma} + h.c.) ,$$

where ϵ_{dm} are the energies of the 4f orbitals and V_m the hybridization matrix element of the local orbital m with the conduction band, $m = 1, \dots, 7$. The resulting generalized NCA equations follow as,

$$\Sigma_{fmm'\sigma}(\omega) = \Gamma_{mm'} \int \frac{d\varepsilon}{\pi} f(\varepsilon) A_{c\sigma}^0(-\varepsilon) G_b(\omega + \varepsilon) \quad (13)$$

$$\Sigma_b(\omega) = \sum_{mm'\sigma} \Gamma_{m'm} \int \frac{d\varepsilon}{\pi} f(\varepsilon) A_{c\sigma}^0(\varepsilon) G_{fmm'\sigma}(\omega + \varepsilon) \quad (14)$$

$$G_{dmm'\sigma}(\omega) = \int d\varepsilon e^{-\beta\varepsilon} [G_{fmm'\sigma}(\omega + \varepsilon) A_b(\varepsilon) - A_{fmm'\sigma}(\varepsilon) G_b(\varepsilon - \omega)] , \quad (15)$$

where $\Gamma_{mm'} = \pi N_0 V_m^* V_{m'}$, and $G_{fmm'\sigma}$, $G_{dmm'\sigma}$ are the matrix generalizations of Eq. (4) associated with the selfenergy matrix $\Sigma_{fmm'\sigma}$ in local orbital space. The fact that there are several single-particle levels at high energies, ϵ_{fm} , grouped together in SO and CF multiplets, implies a rich structure in the low-energy spectrum as well, because fluctuations of an electron from one local orbital via the conduction band to another local orbital are possible in second order in V_m . Since there may be a spin flip involved, these fluctuations induce Kondo-like, logarithmic divergencies in perturbation theory, how-

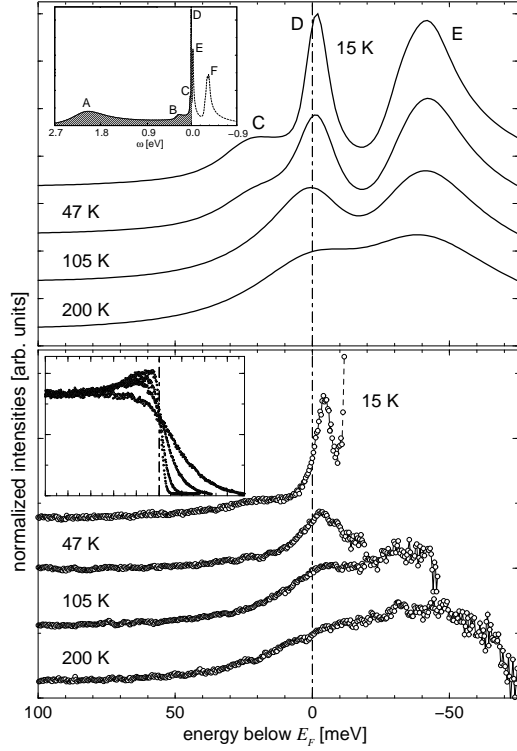


Fig. 2. Upper panel: Theoretical T dependence of the 4f spectral function of CeCu_2Si_2 for $T = 15$ K, 47 K, 105 K, and 200 K. The inset shows the calculated spectrum at $T = 15$ K. Model parameters: $\epsilon_{f1} = -2.4$ eV, CF splittings of the $J = 5/2$ sextet $\Delta_{CF} = 30$ meV and 36 meV, SO splitting $\Delta_{SO} = 270$ meV, hybridization $V = 200$ meV. Lower panel: Photoemission spectra for the same temperatures. The experimental photoemission spectra, divided by the Fermi distribution to gain access to the states above the Fermi energy. The inset shows the raw data on the same energy scale prior to the division. All spectra are normalized to the same intensity at ≈ 100 meV and are offset for clarity.

ever located at energies corresponding to the differences $\Delta\epsilon_{m1} = \epsilon_{fm} - \epsilon_{f1} > 0$ between an excited and the ground state local level, as can be seen, e.g., by inserting the bare pseudofermion Green's function $G_{fmm\sigma}$ in Eq. (14). As a result, there appear (in addition to the central Kondo resonance at the Fermi level), multiple many-body resonances at elevated energies $\Delta\epsilon_{m1}$ given by the SO and CF splittings, as well as shadow peaks at negative energies $-\Delta\epsilon_{m1}$, the so-called SO and CF satellites. The height of these resonances depends roughly logarithmically on T , characteristic of Kondo behavior. In addition, the SO and CF satellites are broadened by the lifetime associated with the inelastic decay of the excited local orbitals. The shadow peaks often appear merely as shoulders in the spectrum, as they correspond to transitions from an only virtually occupied excited 4f orbital into the ground state orbital. This physics has been analyzed analytically in Ref.³⁶ and is qualitatively well captured by the NCA, as a perturbative expansion of Eqs. (13–15) shows. The results of the numerical evaluation of the NCA equations for the impurity spectrum $\frac{1}{\pi}\text{tr}_m [\text{Im}G_{d\sigma}(\omega - i0)]$ are shown in Fig. 2 in comparison to the photoemission spectra of Ref.³⁵ The central Kondo Peak D and the CF satellites (peaks E and shoulders C) with CF splittings

of 30 meV and 36 meV are clearly visible in the main panels. The inset of the upper panel displays the NCA spectrum on a larger energy scale, showing the SO satellites (B and F) with a SO splitting ≈ 360 meV as well as the single-particle resonances A, whose SO and CF splittings are not resolved due to the large lifetime broadenings $\Gamma_{mm'}$. The T dependence agrees qualitatively well with the photoemission spectra in the experimentally accessible temperature range of $T \gtrsim T_K$.

5. Finite- U Anderson impurities: SUNCA

For many quantum impurity problems, including the DMFT treatment of correlated lattice electron systems with a Mott-Hubbard metal-insulator transition, the large, but finite on-site Coulomb repulsion U is essential. However, a naive generalization of the NCA for finite U , the generating functional comprised of the two diagrams in the first line of Fig. 3, does not even give the correct Kondo scale for this problem. The reason is that in this NCA the fluctuations into the empty (“light” bosons b) and into the doubly occupied (“heavy” bosons a) impurity state are not treated symmetrically. The latter is, however, essential to obtain the correct spin exchange coupling

$$J = \frac{|V|^2}{|\epsilon_d|} + \frac{|V|^2}{|\epsilon_d + U|} \quad (16)$$

via a Schrieffer-Wolff transformation.¹⁶ Thus, the asymmetric treatment of either of the two contributions to J leads to a T_K which may be off by an exponentially large factor $\sim e^{\pi|\epsilon_d|/2\Gamma}$ or $\sim e^{\pi|\epsilon_d+U|/2\Gamma}$, i.e. possibly by several orders of magnitude. For a correct treatment of both terms, there must be included, for each diagram with a light boson line, the corresponding diagram with the light boson replaced by a heavy boson line (which amounts to the exchange diagram of the former), and vice versa, *on the level of bare perturbation theory*.^{29,38} The importance of these vertex corrections has first been recognized by Sakai et al.³⁷ and later by Pruschke and Grewe,³⁹ without, however, formulating a conserving approximation. In these works a numerical evaluation has only been given in lowest order (the terms denoted UNCA in Fig. 3). On

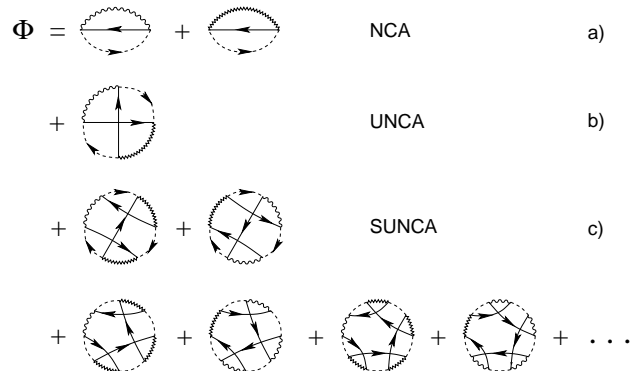


Fig. 3. Generating functional of the SUNCA. Zig-zag lines denote the propagators for doubly occupied or “heavy” bosons. The diagrams a) define the NCA for finite U , the sum of diagrams a) and b) the UNCA, which gives a symmetrical treatment of b and a lines to leading order only.

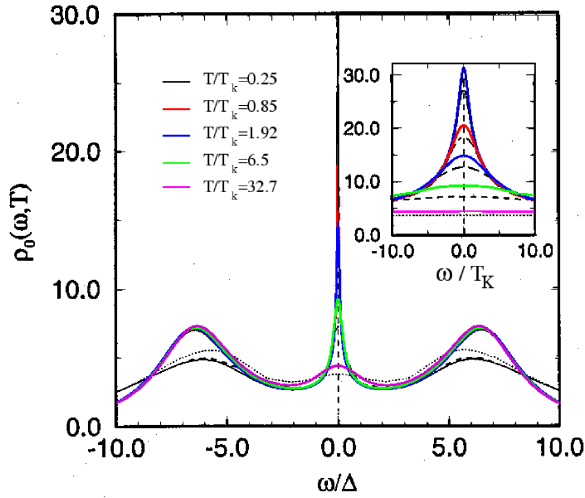


Fig. 4. d -electron spectral function for $U = -2\epsilon_d$. Solid lines: SUNCA results,²⁹ dashed lines: NRG results.⁴⁰

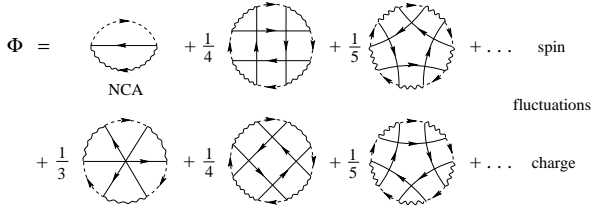


Fig. 5. Diagrammatic representation of the Luttinger-Ward functional generating CTMA. The terms with the conduction electron lines running clockwise (labelled “spin fluctuations”) generate T^{cf} , while the terms with the conduction electron lines running counter-clockwise (labelled “charge fluctuations”) generate T^{cb} (Fig. A-1, see text). The two-loop diagram is excluded, because it is not a skeleton.

the level of renormalized perturbation theory, it means that for each dressed b -line there must be included a ladder vertex function with a -lines as rungs, and vice versa. The generating functional of the corresponding conserving approximation, the so-called Symmetrized Finite-U NCA (SUNCA), is shown in Fig. 3.²⁹ The SUNCA is tractable with relatively moderate numerical effort, since it can be formulated in terms of no higher than 3-point vertex functions. The results of a fully selfconsistent evaluation of the d -electron spectral function within SUNCA are shown in Fig. 4 in comparison with NRG results. It is seen that the correct Kondo scale (width of the Kondo peak) is reproduced. However, the SUNCA solution still develops a spurious low- T singularity. This problem can be cured only by a more sophisticated approximation, the CTMA.

6. Conserving T-Matrix Approximation

To overcome the failures of the NCA to describe the (FL) strong coupling fixed point of the single-channel Anderson model, described in section 3, we have proposed early on the CTMA.¹⁹ Before we present the explicit results of the CTMA, we give the line of arguments that led to the construction of the generating functional of the CTMA.

6.1 Construction of the CTMA

As a minimal precondition to obtain a gauge symmetric description of the FL fixed point, a conserving approximation must reproduce the correct pseudoparticle infrared exponents, Eqs. (6-8), whose dependence on n_d is characteristic for a FL ground state. It is easily seen by power counting arguments that any summation of a finite number of skeleton selfenergy diagrams merely reproduces the incorrect NCA exponents.²⁸ Hence, the generating functional must be comprised of an *infinite* class of skeleton diagrams in order to describe FL behavior, in contrast to the Post-NCA considered by Anders (diagrams up to $O(\Gamma^4)$ in Fig. 5).³¹ Since the latter is a consequence of the singlet state formed at low T between the the impurity and the conduction electron spins, one may expect that higher than two-particle correlation functions need not be considered in the single-channel case. The approximations to the total vertex functions between conduction electrons (c) and impurity degrees of freedom (pseudofermions f , slave bosons b) are then two-particle T-matrices. As the irreducible parts of these T-matrices we select the single (renormalized) b or f particle lines, since (1) in the Kondo regime these terms are the leading contributions in the small parameter VN_0 ; and (2), in the spirit of principal diagrams, this choice gives rise to the maximum number of spin and charge fluctuation processes in the T-matrices at any given order of (renormalized) perturbation theory. This choice results in the ladder approximations T^{cf} , T^{cb} for the total two-particle vertices shown in Fig. A-1 (2), (3). The Luttinger-Ward functional generating these ladder vertex terms (and others) is shown in Fig. 5. It is comprised of all closed pseudoparticle rings (skeletons) with each conduction electron line spanning at most two hybridization vertices and has been termed the “Conserving T-Matrix Approximation” (CTMA). The pseudofermion and slave boson selfenergies, derived by functional derivative, are shown in Fig. 6. Note that the vertex equations for T^{cf} , T^{cb} , coupled via the selfenergies, have parquet character. The analytical expressions for $\Sigma_{f\sigma}$, Σ_b and $G_{d\sigma}$ are given explicitly in Ref.^{30,32}

The selfconsistent CTMA equations are solved numerically by iteration. The results shown below support strongly that the CTMA correctly describes the strong coupling FL regime of the single-channel Anderson im-

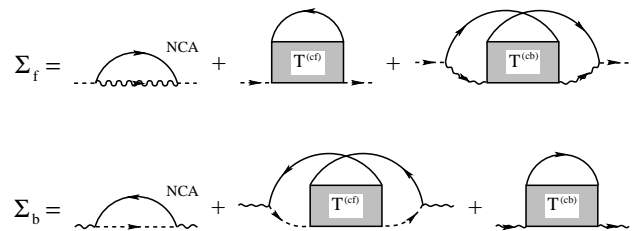


Fig. 6. The CTMA pseudofermion and slave boson selfenergies. In the second diagram of $\Sigma_{f\sigma}$ and the third diagram of Σ_b the 1- and 2-rung contributions, and in the third diagram of $\Sigma_{f\sigma}$ and the second diagram of Σ_b the 1-rung contribution to the respective T-matrices are omitted, (not shown explicitly), in order to avoid double counting.

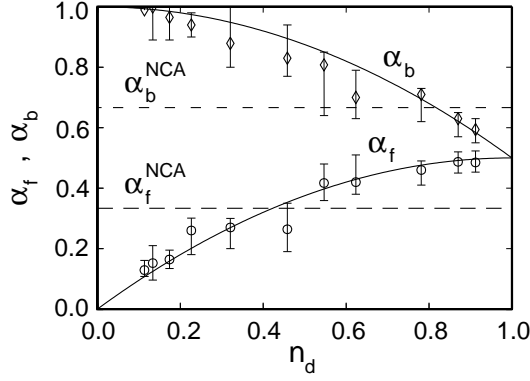


Fig. 7. CTMA results (symbols with error bars) for the threshold exponents α_f and α_b of $A_{f\sigma}$ and A_b for $U \rightarrow \infty$, $B = 0$. Solid lines: exact values, Eqs. (6,7), dashed lines: NCA results.

purity model. In the appendix evidence is provided that it also systematically describes the high-energy regime above T_K .

6.2 Results

Pseudoparticle spectral functions. As a first indication for description of FL behavior within CTMA it has been checked if the CTMA reproduces the correct FL values of the pseudoparticle threshold exponents.¹⁹ The exponents were obtained by a fit to the numerical low- T solutions for $A_{f\sigma}$, A_b in a log-log plot. The results are shown in Fig. 7, showing, within the error bars, good agreement with the exact values and especially the dependence on the impurity occupation number n_d , characteristic for the FL fixed point.

The static spin susceptibility of the impurity was calculated from the spin dependent occupation numbers $n_{d\sigma}$ in a magnetic field B as,

$$\chi_i(T) = \left. \frac{dM}{dB} \right|_{B=0} \quad (17)$$

where $M = g\mu_B \sum_{\sigma} \sigma n_{\sigma}$ is the impurity magnetization and

$$n_{d\sigma} = \lim_{\lambda \rightarrow \infty} \frac{\int d\omega e^{-\beta\omega} \text{Im} G_{f\sigma}(\omega - i0)}{\int d\omega e^{-\beta\omega} \text{Im} [\sum_{\sigma} G_{f\sigma}(\omega - i0) + G_b(\omega - i0)]}. \quad (18)$$

$\chi_i(T)$ shows T -independent Pauli behavior for $T \lesssim 0.5T_K$ and down to the lowest T considered,³² indicative of the FL ground state with a completely screened local moment (Fig. 8). As expected, $\chi_i(T)$ obeys scaling for at least a range of T_K within a factor 10,⁴¹ when plotted as a function of T/T_K and in units of $(g\mu_B)^2/(4T_K^*) \equiv \chi_i(T=0)/W$, where $W = T_K^*/T_L$ is the universal Wilson number and T_K^* is Wilson's original definition of T_K .³ Since the BA and selfconsistent perturbation theory use somewhat different definitions of T_K , we rescale the latter in the CTMA as well as in the BA solution such that it coincides with T_K^* . This allows for a quantitative comparison of BA and CTMA and for a determination of the CTMA approximation to W . The result is shown in Fig. 8, exhibiting remarkably good quantitative agreement. We obtain $W^{(CTMA)} \simeq 0.462$ as compared to the exact result $W \simeq 0.4128$.

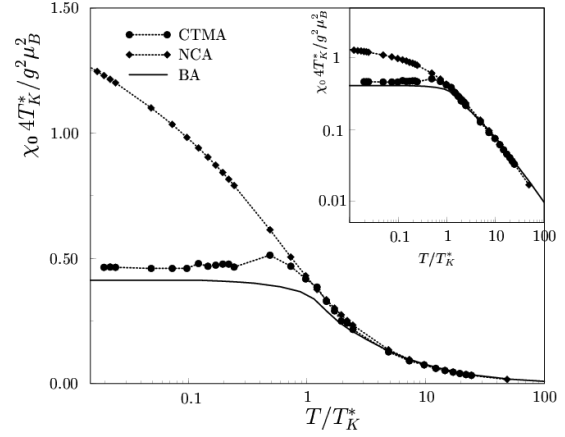


Fig. 8. Static spin susceptibility as a function of temperature; BA, CTMA and NCA results (see text). Model parameters used: $\epsilon_d/D = -0.81$, $\Gamma/D = 0.2$.

FL behavior of the *impurity electron spectral function* $A_{d\sigma}(\omega)$ and *selfenergy* $\Sigma_{d\sigma}(\omega)$ is of prime interest especially for applications within DMFT. The imaginary part of the impurity electron interaction selfenergy $\Sigma_{d\sigma}(\omega - i0)$, calculated in CTMA³² from

$$G_{d\sigma}(\omega) = [\omega - \epsilon_d - i\Gamma - \Sigma_{d\sigma}(\omega)]^{-1}, \quad (19)$$

is shown in Fig. 9. $\Sigma_{d\sigma}$ exhibits many features of FL behavior. It has quadratic dependence on both, ω and T , at low ω , T , with no sign of a spurious low-energy singularity down to the lowest T considered ($T \simeq 0.01 T_K$). As discussed in detail in Ref.,³² the curvature of the quadratic behavior in ω and T is found to be in good agreement with the exact FL result, $\Sigma_{d\sigma}(\omega) = a[\omega^2 + (\pi T)^2]/T_K^2$, where a is an exactly known prefactor.^{32, 42} However, the position ω_0 of the minimum of $\text{Im}\Sigma_{d\sigma}(\omega)$

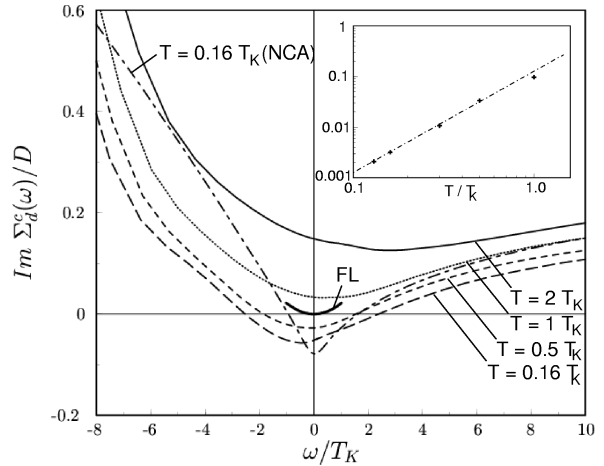


Fig. 9. Imaginary part of the CTMA impurity electron selfenergy $\text{Im}\Sigma_{d\sigma}(\omega)$ for various T for the same parameters as in Fig. 8. The small solid arch represents the exact FL behavior at $T = 0$.³² The NCA result at $T = 0.16T_K$ is shown for comparison. Inset: the T dependence of the minimum value of $\text{Im}\Sigma_{d\sigma}$ (black dots). The dashed-dotted line, drawn for comparison, has slope 2.

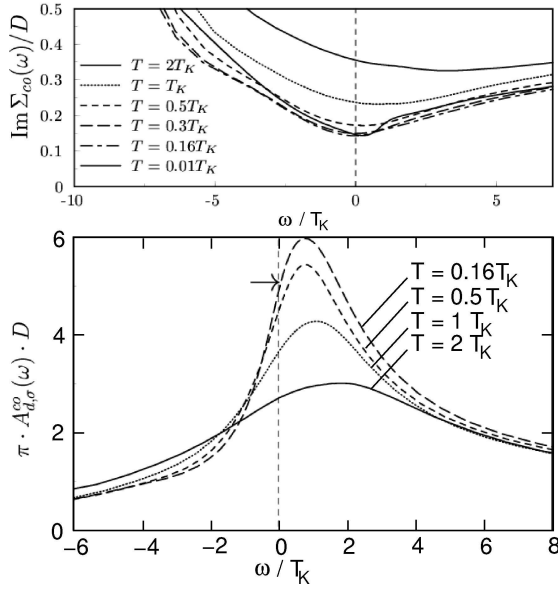


Fig. 10. d -electron selfenergy $\Sigma_{d\sigma}(\omega)$ and spectral function $A_d(\omega)$ after the potential scattering correction has been applied (see text). The arrow (lower panel) marks the unitarity sum rule.

is incorrectly shifted to $\omega_0 \approx -T_K$, and $\text{Im}\Sigma_{d\sigma}(\omega - i0)$ acquires negative values, thus violating the Friedel sum rule. When searching for the origin of this shortcoming, one must keep in mind that $\Sigma_{d\sigma}(\omega \approx 0)$ is determined via Eq. (19) by both $\text{Im}G_{d\sigma}(\omega)$ and $\text{Re}G_{d\sigma}(\omega)$, and thus, through the Kramers-Kronig relation, by high-energy (potential scattering) contributions to $A_{d\sigma}(\omega)$. Hence, the erroneous shift ω_0 may result from an unprecise calculation of $G_{d\sigma}(\omega)$ at high energies, either numerically or due to neglect of high-order potential scattering terms.⁴³ To correct this shortcoming, it has been suggested to add an appropriate, phenomenological *real constant* to $\Sigma_{d\sigma}(\omega)$. Through selfconsistency it acts like a chemical potential and shifts the minimum of $\text{Im}\Sigma_{d\sigma}(\omega)$ to $\omega = 0$. The results of this correction are shown in Fig. 10. It is seen that by a single, real parameter, motivated by potential scattering contributions, the full FL behavior of $\Sigma_{d\sigma}(\omega)$ is recovered, and $A_d(\omega)$ obeys the unitarity sum rule with good precision.

7. Conclusions

We have reviewed the method of conserving auxiliary particle approximations for quantum impurities with strong onsite repulsion U . We have shown that on the level of generalized NCA relatively easily tractable approximations are possible which give a qualitatively correct description of, e.g., Anderson impurities with multiple orbitals or finite U (SUNCA) at not too low temperature, but invariably fail in the strong coupling regime below T_K as well as in a magnetic field. It was shown, both by numerical solutions and by a perturbative RG analysis, that the CTMA, although numerically demanding, provides a remedy for all of these failures, and gives an essentially correct description of the FL behavior in the Anderson impurity model. It remains to be investigated if this makes the CTMA a suitable “impurity solver” within the DMFT approach to correlated lattice

problems.

We are grateful for useful discussions with S. Kirchner, K. Haule, T. A. Costi, A. Rosch, H. Keiter, G. Kotliar and G. Sellier. Parts of this work have been done in collaboration with K. Haule, T. A. Costi, and, in particular, S. Kirchner. We acknowledge the hospitality of the Aspen Center for Physics, where this paper has been completed. This work is supported in part by the DFG and by a Max-Planck Research award (P.W.).

Appendix: Perturbative RG analysis

As seen in section 6, conserving approximations provide a means for selecting the physically essential contributions even in the strong coupling regime, while preserving the symmetries of the problem. However, because of the selfconsistent resummation it is non-trivial to find an approximation which also includes the leading logarithmic terms at each order of *bare* perturbation theory. The latter is known to provide a quantitatively correct description of physical quantities in the weak and intermediate coupling regime, i.e. as long as $\ln(\max[T, \omega]/T_K) \gtrsim 1$. On the other hand, the leading log summation is equivalent to the perturbative coupling constant RG in the sense specified below. For finding the proper conserving approximation it is, therefore, useful to have a method which allows to analyze whether or not the approximation reproduces the correct weak coupling RG flow of the effective coupling constants under high-energy cut-off rescaling. In this appendix we present such a method and apply it to the NCA and to the CTMA for the Anderson model in the Kondo regime for $U \rightarrow \infty$.

The coupling constant RG starts from the observation that in a renormalizable system, like the Kondo problem, where the T, ω and B dependence of physical quantities χ is characterized by a single low-energy scale T_K (i.e. given by a universal function of the dimensionless variables $T/T_K, \omega/T_K, B/T_K$ etc.), these quantities must be invariant under high-energy cut-off rescaling $D \rightarrow D - dD$, and so must the two-particle vertex functions, the physical quantities are comprised of. Hence, the direct calculation of χ is replaced by the renormalization of the vertex operators Λ of the Hamiltonian such as to keep the total (fully reducible) vertex functions γ^{cf} (spin and potential scattering) and γ^{cb} (potential scattering) invariant under cut-off rescaling, and subsequent calculation of χ to leading order bare perturbation theory in the renormalized couplings. The same RG scheme can be applied, if χ is not given exactly, but in some conserving approximation. In this case, one must identify the approximate γ^{cf}, γ^{cb} as dictated by the approximation for χ . Hence, the RG analysis of a conserving approximation amounts to the

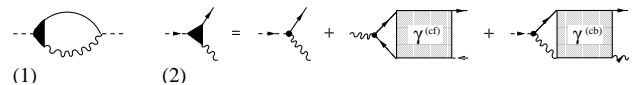


Fig. 11. (1) Pseudofermion selfenergy expressed in terms of the exact 3-point vertex \hat{V} (black triangle). (2) Representation of \hat{V} in terms of the 4-point vertices γ^{cf}, γ^{cb} . The first diagram on the right-hand side is the bare 3-point vertex V . The pseudofermion-slave boson vertex γ^{fb} vanishes by the projection onto $Q = 1$.

following procedure,⁴⁵ see also:⁴⁶

(1) *Determination of the approximate vertex functions.* In any approximation, a physical quantity can be expressed in terms of the full hybridization vertex \tilde{V} and of bare Green's functions, the latter being RG invariant by definition, e.g. the f selfenergy (Fig. 11 (1)),

$$\Sigma_{f\sigma}(\omega) = V \int \frac{d\varepsilon}{2\pi} f(\varepsilon) G_b^0(\varepsilon + \omega - i0) \times \quad (\text{A.1})$$

$$[\tilde{V}(\omega, \varepsilon + i0) G_{c\sigma}^0(-\varepsilon - i0) - \tilde{V}(\omega, \varepsilon - i0) G_{c\sigma}^0(-\varepsilon + i0)].$$

\tilde{V} , in turn, is composed of four-point vertex functions as shown in Fig. 11 (2). This defines the approximate γ^{cf} , γ^{cb} . Note that only for a conserving approximation this definition is unique, independent of the physical quantity considered.

(2) *Bare perturbation theory for γ^{cf} , γ^{cb} .* Due to the conserving method, the four-point vertex functions are comprised of the dressed propagators. In order to perform the perturbative RG, these must be written out in bare perturbation theory (non-skeleton diagrams). In leading log approximation, there are two significant simplifications: (i) Each contribution to the pseudofermion self-energy contains at least one integration over the slave boson propagator G_b (compare, e.g. Eq. (9)). Its logarithmic contribution is cut off at high energies $\omega \gg T_K$ by the pole in $G_b(\omega)$ at $\omega \approx \epsilon_d$. Note that this remains true even for the dressed G_b . Hence, only the bare pseudofermion Green's function appears in γ^{cf} , γ^{cb} . (ii) Self-energy insertions to propagators which are integrated over in γ^{cf} , γ^{cb} are of subleading order and should, therefore, be neglected.

(3) Perform on the terms obtained in this way the perturbative cut-off rescaling scheme^{2,42} to obtain the RG equations for the spin and potential scattering coupling constants.

A.1 Perturbative RG for the NCA

Considering the NCA selfenergies in Fig. 1 (or the NCA d-electron Green's function) and following the steps (1), (2) above, γ^{cf} is identified as the full slave boson propagator, $\gamma_{s'\sigma',s\sigma}^{cf} = |V|^2 G_b$, i.e. by the expression given diagrammatically by Fig. A.1 (1). The conduction electron-slave boson vertex function γ^{cb} is by construction proportional to the unit matrix in spin space since the slave bosons don't carry spin, and can only give potential scattering contributions. Within NCA, it is $\gamma_{s',s}^{cb} = |V|^2 G_{f\sigma} \delta_{ss'} \delta_{ss'}$, i.e. of subleading order. Performing the cut-off rescaling $D \rightarrow D - dD$ on γ^{cf} , one arrives, to first order in dD and in leading logarithmic approximation, at the correction to the irreducible c - f vertex,

$$d\Lambda_{s'\sigma',s\sigma}^{cf,(1)} = -N_0 \frac{dD}{D} \sum_{s''\sigma''} [\Lambda^{(cf)}]_{s'\sigma',s''\sigma} [\Lambda^{(cf)}]_{s''\sigma',s\sigma''},$$

with the spin indices as defined in Fig. A.2 (1). The dot in Fig. A.2 indicates that the integration over the conduction electron energy is restricted to the infinitesimal range $[-D, -D + dD]$, $[D - dD, D]$.

Λ^{cf} , $\delta\Lambda^{cf}$ are matrices in the product space of the pseudofermion and conduction electron spins, and,

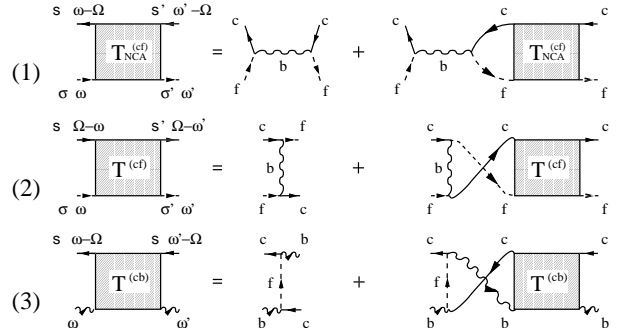


Fig. A.1. Diagrammatic representation of the Bethe-Salpeter equations for (1) the NCA approximation to the fully reducible conduction electron-pseudofermion p-h vertex $\gamma_{NCA}^{(cf)}$ (2) the c - f T-matrix T^{cf} , and (3) the c - b T-matrix T^{cb} . The CTMA approximation to γ^{cf} is the sum of (1) and (2). For the perturbative RG, all single-particle propagators are understood to be the bare ones (see text). The external lines are drawn for clarity and do not belong to the vertices. Single-particle reducible parts (SPRs) in (2) are omitted, since the SPRs of the total c - f vertex do not contribute to the RG flow because of rule (i) (see text).

hence, can be decomposed into spin flip, $J_{\perp} (S^+ \otimes \sigma^- + S^- \otimes \sigma^+)$, spin z-component, $J_{\parallel} (S_z \otimes \sigma_z)$, and potential scattering, $W (\mathbf{1} \otimes \mathbf{1})$, contributions, where S^{\pm} , σ^{\pm} are the impurity and the conduction electron spin flip operators, and S_z , σ_z the z-components of the impurity spin and the conduction electron Pauli matrices, respectively. J_{\perp} , J_{\parallel} , W are the respective running coupling constants, with $J_{\perp} = J_{\parallel} = 2W \equiv |V|^2 G_b^0(\omega) = |V|^2 / |\epsilon_d|$ for $\omega \ll |\epsilon_d|$ for the Anderson model. This decomposition leads to the perturbative RG equations for the coupling constants within NCA,

$$\frac{dJ_{\perp}}{d\ln D} = -N_0(J_{\parallel}J_{\perp} + 2WJ_{\perp}) \quad (\text{A.2})$$

$$\frac{dJ_{\parallel}}{d\ln D} = -N_0(J_{\perp}^2 + 2WJ_{\parallel}) \quad (\text{A.3})$$

$$\frac{dW}{d\ln D} = -N_0\left(\frac{1}{2}J_{\perp}^2 + \frac{1}{4}J_{\parallel}^2 + W^2\right). \quad (\text{A.4})$$

Eqs. (A.2–A.4) reveal two remarkable facts. (1) Within NCA the potential scattering amplitude W is erroneously renormalized under the RG flow, leading to a spurious divergence of W . (2) The RG equations are easily integrated to give (J_0 is the bare coupling),

$$J(D) = \frac{J_0}{1 + 2N_0J_0\ln\frac{D}{D_0}}, \quad (\text{A.5})$$

i.e. the spin coupling constant J as well as the potential scattering amplitude W diverge at the Kondo temperature $T_K = D_0 e^{-1/(2N_0J_0)}$. This demonstrates that for $U \rightarrow \infty$ the NCA reproduces the Kondo scale correctly, however due to an accidental cooperation of spin and potential scattering terms.

One may conjecture that this fact, that the NCA does not distinguish between potential and spin scattering, is the origin why the NCA gives a qualitatively incorrect description of the Kondo resonance in a magnetic field, see section 3: While the divergent spin scattering amplitude depends on magnetic field and leads to the

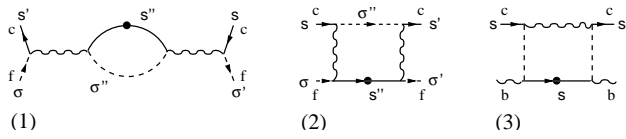


Fig. A-2. Perturbative RG renormalizations of the (irreducible) c-f vertex. Diagram (1) is the NCA result, the sum of diagrams (1), (2), (3) is the result of CTMA, where (3) is the contribution from the c-b vertex, which is not scaling and is neglected. The black dots on the conduction electron lines indicate that the frequency integrals in those lines are restricted to the regions $[-D, -D + dD]$, $[D, D - dD]$.

correct Zeeman splitting of the Kondo resonance,⁴⁴ the incorrectly diverging potential scattering term is insensitive to the magnetic field and leads to the spurious third peak produced by the NCA at $\omega = 0$ at finite magnetic field.

A.2 Perturbative RG for the CTMA

We now consider the coupling constant renormalization under the RG flow within CTMA. From the analysis of the selfenergies shown in Fig. 6 and of the corresponding $G_{d\sigma}$ the CTMA approximation for γ^{cf} is given by the sum of the contributions shown in Fig. A-1 (1), (2). The contribution Fig. A-1 (2) leads to an additional c-f vertex renormalization under cutoff reduction, shown in Fig. A-2 (2),

$$d\Lambda_{s'\sigma',s\sigma}^{cf,(2)} = +N_0 \frac{dD}{D} \sum_{s''\sigma''} [\Lambda^{(cf)}]_{s'\sigma',s''\sigma''} [\Lambda^{(cf)}]_{s''\sigma'',s\sigma},$$

The contribution Fig. A-1 (3) leads to the c-b vertex renormalization shown in Fig. A-2 (3), which, as a pure potential scattering term is not scaling, and, therefore, neglected. Adding $d\Lambda^{cf,(1)}$ and $d\Lambda^{cf,(2)}$ and decomposing into J_{\perp} , J_{\parallel} and W contributions, one obtains the RG equations of CTMA,

$$\frac{dJ_{\perp}}{d\ln D} = -2N_0 J_{\parallel} J_{\perp} \quad (\text{A-6})$$

$$\frac{dJ_{\parallel}}{d\ln D} = -2N_0 J_{\perp}^2 \quad (\text{A-7})$$

$$\frac{dW}{d\ln D} = 0. \quad (\text{A-8})$$

Inspection of the two terms in Fig. A-2 shows that they are the direct (2) and the exchange (1) scattering contributions and, upon collapsing the bare boson lines for $\omega \ll |\epsilon_d|$ to the spin coupling, $-|V|^2 G_b^0(\omega) \rightarrow -|V|^2/\epsilon_d = J$, that they directly correspond to the two well-known contributions to the perturbative one-loop β -function of the Kondo problem.^{2,42} The failure of the NCA in the weak coupling regime is, thus, traced back to the fact that it incorporates only the exchange term, and the direct term is missing. This is cured by the CTMA: The RG equations (A-6–A-8) are identical to the well-known perturbative RG equations of the original Kondo model. This proves that the CTMA incorporates the complete Kondo physics also in the weak and intermediate coupling regime, where the perturbative RG is valid. One may expect that, as a consequence, the CTMA correctly

describes the Zeeman-like splitting of the Kondo resonance in a magnetic field, since it is quantitatively correct for the susceptibility as well (see section 6).

- 1) J. Kondo: Progr. Theor. Phys. **32** (1964) 37; Solid State Physics **23** (1969) 184.
- 2) P.W. Anderson: J. Phys. C **3** (1970) 2439.
- 3) K.G. Wilson: Rev. Mod. Phys. **47** (1975) 773.
- 4) N. Andrei: Phys. Rev. Lett. **45** (1980) 379.
- 5) P.B. Wiegmann: Sov. Phys. JETP Lett. **31** (1980) 392.
- 6) A. Georges, G. Kotliar, W. Krauth, M. J. Rozenberg: Rev. Mod. Phys. **68** (1996) 13.
- 7) P.W. Anderson: Phys. Rev. **124** (1961) 41.
- 8) D. Goldhaber-Gordon et al.: Nature **391** (1998) 156; S. M. Cronenwett, T. H. Oosterkamp, L. P. Kouwenhoven: Science **281** (1998) 540; J. Schmid et al.: Physica **B258** (1998) 182.
- 9) J. Nygård, D. H. Cobden, and P. E. Lindelof: Nature **408** (2000) 342; M. R. Buitelaar, T. Nussbaumer, C. Schönenberger, Phys. Rev. Lett. **89** (2002) 256801.
- 10) D. C. Ralph, R. A. Buhrman: Phys. Rev. Lett. **72** (1994) 3401.
- 11) J. Park et al.: Nature **417** (2002) 722.
- 12) J. Kroha, A. Zawadowski: Phys. Rev. Lett. **88** (2002) 176803.
- 13) R. Aguado, D. C. Langreth: Phys. Rev. B **67**, (2003) 245307.
- 14) A. A. Abrikosov: Physica **2** (1965) 5.
- 15) S. E. Barnes: J. Phys. **F6** (1976) 1375; **F7** (1977) 2637.
- 16) J.R. Schrieffer, P.A. Wolff: Phys. Rev. **149** (1966) 491.
- 17) T.A. Costi, J. Kroha, P. Wölfle: Phys. Rev. **B 53** (1996) 1850.
- 18) B. Menge, E. Müller-Hartmann: Z. Phys. **B 73** (1988) 225.
- 19) J. Kroha, P. Wölfle, T.A. Costi: Phys. Rev. Lett. **79** (1997) 261.
- 20) T.A. Costi, Schmitteckert, J. Kroha, P. Wölfle: Phys. Rev. Lett. **73** (1994) 1275; Physica **C235-240** (1994) 2287.
- 21) G. Baym, L. P. Kadanoff: Phys. Rev. **124** (1961) 287; G. Baym: Phys. Rev. **127** (1962) 1391.
- 22) H. Keiter, J.C. Kimball: Int. J. Magn. **1** (1971) 233.
- 23) N. Grewe, H. Keiter: Phys. Rev. B **24** (1981) 4420.
- 24) Y. Kuramoto: Z. Physik **B 53** (1983) 37.
- 25) H. Kojima, Y. Kuramoto, M. Tachiki: Z. Physik **B 54** (1984) 293; Y. Kuramoto, H. Kojima: Z. Physik **57** (1984) 95; Y. Kuramoto: Z. Physik **B 65** (1986) 29.
- 26) N.E. Bickers, D.L. Cox, J. W. Wilkins: Phys. Rev. **B 36** (1987) 2036; N.E. Bickers: Rev. Mod. Phys. **59** (1987) 845.
- 27) E. Müller-Hartmann: Z. Physik **B 57** (1984) 281; Y. Kuramoto, E. Müller-Hartmann: J. Mag. Mag. Mat. **57** (1985) 122.
- 28) D.L. Cox, A.R. Ruckenstein: Phys. Rev. Lett. **71** (1993) 1613.
- 29) K. Haule, S. Kirchner, J. Kroha, P. Wölfle: Phys. Rev. **B 64** (2001) 155111.
- 30) J. Kroha, P. Wölfle: in Theoretical Methods for Strongly Correlated Electrons, CRM Series in Mathematical Physics, Springer, New York (2003) 297.
- 31) F. B. Anders, N. Grewe: Europhys. Lett. **26**, (1994) 551.
- 32) S. Kirchner, J. Kroha, P. Wölfle: Phys. Rev. B **70** (12) (2004) in press; cond-mat/0404311.
- 33) Th. Maier et al.: Phys. Rev. Lett. **85** (2000) 1524.
- 34) G. Kotliar et al.: Phys. Rev. Lett. **87** (2001) 186401.
- 35) F. Reinert et. al.: Phys. Rev. Lett. **87** (2001) 106401.
- 36) J. Kroha et. al.: Physica E **18** (2003) 69.
- 37) O. Sakai, M. Motizuki, T. Kasuya: Springer Series in Solid-State Sciences **81**, (Springer, 1988) 45.
- 38) J. Holm, K. Schönhammer: Solid State Comm. **69** (1989) 969.
- 39) Th. Pruschke, N. Grewe: Z. Phys. **B 74** (1989) 439.
- 40) We are grateful to T. A. Costi for providing the NRG data.
- 41) J. Kroha, P. Wölfle: unpublished.
- 42) A. C. Hewson: *The Kondo Problem to Heavy Fermions*, Cambridge University Press, Cambridge, England (1993).
- 43) Note, however, that CTMA includes all potential scattering terms up to $O(\Gamma^4)$.
- 44) A. Rosch, J. Paaske, J. Kroha, P. Wölfle, Phys. Rev. Lett. **90** (2003) 076804.
- 45) S. Kirchner, J. Kroha: J. Low Temp. Phys. **126** (2002) 1233.
- 46) E. Lebanon, A. Schiller, V. Zevin, Phys. Rev. B **64** (2001) 245338.